Published in final edited form as:
Nanomedicine (Lond). 2010 November ; 5(9): 1341–1356. doi:10.2217/nnm.10.87.

Detection of macrophages via paramagnetic vesicles incorporating oxidatively tailored cholesterol ester: an approach for atherosclerosis imaging

Andrei Maiseyeu[1], **Georgeta Mihai**[1], **Sashwati Roy**[1,2], **Nisharahmed Kherada**[1], **Orlando P Simonetti**[1], **Chandan K Sen**[1,2], **Qinghua Sun**[1,3], **Sampath Parthasarathy**[1,2], and **Sanjay Rajagopalan**[1,†]

[1] Davis Heart & Lung Research Institute, Room 110, 473 W 12th Avenue, Columbus, OH 43210-1252, USA

[2] Department of Surgery, Colleges of Medicine & Public Health, The Ohio State University, OH, USA

[3] Division of Environmental Health Sciences, Colleges of Medicine & Public Health, The Ohio State University, OH, USA

Abstract

Aim—Macrophages play a key role in the initiation, progression and complications of atherosclerosis. In this article we describe the synthesis of biocompatible, paramagnetic, fluorescent phosphatidylserine vesicles containing cholesterol ester with a free carboxylic acid function and its use for targeted imaging of macrophages.

Methods & results—We synthesized anionic vesicles containing a combination of phosphatidylserine and a novel synthetic oxidized cholesterol ester derivative (cholesterol-9-carboxynonanoate [9-CCN]). *In vitro* studies to characterize particle size, MRI relaxation times and stability were performed. Vesicles containing 9-CCN demonstrated enhanced ability to bind human low-density lipoprotein and to be internalized by macrophages. Experiments in cultured macrophages with 9-CCN vesicles, alone and in the presence of low-density lipoprotein, indicated uptake of vesicles through scavenger receptor and integrin-dependent pathways. *In vivo* MRI using 9-CCN vesicles containing gadolinium in a rabbit model of atherosclerosis revealed protracted enhancement of 9-CCN vesicles and colocalization with arterial macrophages not seen with control vesicles. Pharmacokinetic experiments demonstrated prolonged plasma residence time of 9-CCN vesicles, perhaps due to its capacity to bind to low-density lipoprotein.

†Author for correspondence: Tel.: +1 614 247, 2532 Fax: +1 614 688 4233, Sanjay.Rajagopalan@osumc.edu.

Ethical conduct of research
The authors state that they have obtained appropriate institutional review board approval or have followed the principles outlined in the Declaration of Helsinki for all human or animal experimental investigations. In addition, for investigations involving human subjects, informed consent has been obtained from the participants involved.

Financial & competing interests disclosure
This work was partially supported by RO1 ES015146 and R21 DK088522. Sashwati Roy is supported by NIH RO1 DK076566 and Chandan K Sen is supported by NIH GM 077185. This work was also supported in part by the Davis Heart and Lung Regenerative Medicine Thematic Award; Grant IRG-67–003–44 from the American Cancer Society. The authors would like to acknowledge Heart and Lung Research Institute core facilities for providing Applied Biosystems Q-TRAP LC/MS/MS instrument for this work. The authors have no other relevant affiliations or financial involvement with any organization or entity with a financial interest in or financial conflict with the subject matter or materials discussed in the manuscript apart from those disclosed.
No writing assistance was utilized in the production of this manuscript.

Conclusion—Vesicles containing 9-CCN demonstrate prolonged plasma and plaque retention in experimental atherosclerosis. Such a strategy may represent a simple yet clinically relevant approach for macrophage imaging.

Keywords

atherosclerosis; low-density lipoprotein; magnetic resonance imaging

Imaging of macrophages in atherosclerotic plaque may allow derivation of prognostic information in addition to enabling targeted approaches to ablate or modify macrophage function. Prior studies have established the feasibility of imaging macrophages using contrast agents that incorporate antibodies [1–3], lipoproteins [4–6] and synthetic peptides [4, 7]. Combining affinity with biocompatibility, safety and ease of preparation is essential to any clinically applicable formulation. Recent studies suggest that uptake of apoptotic debris by macrophages is facilitated by specific 'eat-me' signals exteriorized on the plasma membrane surface of apoptotic cells [8, 9]. Phosphatidylserine (PS) and oxidized lipids are pivotal cues in this process [9, 10]. In atherosclerotic plaques, the genesis of foam cells is believed to relate to the engulfment of highly negatively charged oxidatively modified lipoproteins [11, 12]. Cholesteryl or 7-ketocholesteryl esters of 9-oxononanoate represent a frequent type of oxidized lipid present both intracellularly within plaque macrophages and extracellularly in advanced atherosclerotic lesions [13]. We hypothesized that incorporation of PS and cholesteryl-9-carboxynonanoate (9-CCN), two highly anionic lipids, within a lipid-based delivery platform would allow recognition and subsequent uptake by macrophages present in atherosclerotic plaque. Accordingly, in this investigation we describe the synthesis of 9-CCN-containing anionic vesicles that additionally incorporate two different reporter molecules for their MRI and fluorescent detection in atherosclerotic lesions. *In vitro* and *in vivo* evaluation of these vesicles was carried out and compared with control PS vesicles without 9-CCN. Three vesicle formulations were studied: vesicles composed of PS and 9-CCN; vesicles containing PS (control); and vesicles containing PS and 9-CCN-OMe, a methyl ester of 9-CCN. These formulations were termed oxPL, PL and mePL, respectively (Figure 1). The latter has the carboxyl function blocked and, thus, would be expected to be less anionic. All vesicles were formulated with one of the aforementioned lipids in conjunction with paramagnetic gadolinium (Gd) lipid (for MRI detection), vehicle lipid (phosphatidylcholine) and fluorescent (rhodamine) lipid. Gd lipid and oxidatively modified cholesterol lipid (9-CCN) is easily synthesized using a one-step procedures in gram-scale quantities. Use of PS/phosphatidylcholine in approved clinical formulations [14, 15] and ease of synthesis makes such a strategy attractive for scale-up and eventual human use.

Methods

L-α-phosphatidylcholine (from chicken eggs), 1, 2-dioleoyl-sn-dlycero-3-[phospho-L-serine and 1, 2-dioleoyl-sn-glycero-3-phosphoethanolamine-*N*-(lissamine rhodamine B sulfonyl) were purchased from Avanti Polar Lipids Inc. (Alabaster, AL, USA). Cholesterol, azelaic acid and all other chemicals were obtained from Sigma-Aldrich Corporation (St Louis, MO, USA); Gd-diethylenetriaminepentaacetic acid distearylamide (Gd-DTPA-SA) was synthesized according to methods described in [16], RPMI 1640, fetal bovine serum and phosphate-buffered saline (PBS) were purchased from Cellgro Mediatech Inc. (Herndon, VA, USA); penicillin-streptomycin, glutamine and sodium pyruvate were from Gibco/InVitrogen (Carlsbad, CA, USA).

^{1}H and ^{13}C NMR spectra were recorded on a Bruker AVANCE-400 spectrometer. Transmission electron microscopy (TEM) was performed using a FEI Technai G2 Spirit

TEM operating at 80 kV. Samples negatively stained with ammonium molybdate were applied on Formvar-coated copper grids and analyzed.

Mass spectra were acquired in positive ion mode using an Applied Biosystems 3200 QTRAP coupled with electrospray ionization (ESI) source. Capillary temperature was set at 300°C, and spray voltage was set at 5.5 kV. Nebulizer gas and auxiliary gas flow was set to 60 and 20 arbitrary units, respectively. Curtain gas was set to 15.00 and collision gas settings were on medium.

Synthesis of 9-CCN

To a solution of cholesterol (1 g, 2.6 mmol) and azelaic acid (1.4 g, 7.5 mmol) in the 20 ml of mixture of acetone-chloroform (1:1 by volume), *N*-(3-dimethylaminopropyl)-*N*′-ethylcarbodiimide hydrochloride (1.9 g, 10 mmol) and 4-(dimethylamino)pyridine (610 mg, 5 mmol) were added and flushed with nitrogen. The mixture was vigorously stirred overnight, concentrated and purified by column chromatography on silica gel using dichloromethane-methanol mixture as the eluent (9:1 by volume) to give 9-CCN (1.05 g, 74%) as a colorless solid. The product was found to be more than 95% pure by ^{1}H-NMR and high-performance liquid chromatography (HPLC).

^{1}H-NMR (400 MHz, chloroform-d), δ ppm 0.66 (s, 3 H), 0.85 (dd, *J* = 6.6, 1.8 Hz, 4 H), 0.89 (d, *J* = 6.6 Hz, 4 H), 1.00 (s, 3 H), 1.12 (m, 4 H), 1.33 (m, 12 H), 1.49 (s, 6 H), 1.59 (m, 4 H), 1.82 (m, 2 H), 1.98 (m, 2 H), 2.13 (s, 3 H), 2.29 (m, 8 H), 2.99 (s, 2 H), 3.65 (s, 1 H), 4.59 (m, 1 H), 5.35 (d, *J* = 3.8 Hz, 1 H); ^{13}C-NMR (100 MHz, chloroform-d), δ ppm 11.83, 18.69, 19.30, 21.01, 22.53, 22.79, 23.81, 24.26, 24.58, 24.83, 24.86, 26.52, 27.79, 27.98, 28.20, 28.80, 31.75, 31.89, 33.90, 34.61, 35.36, 36.16, 36.98, 38.13, 39.50, 39.72, 42.30, 50.01, 52.36, 56.12, 56.68, 73.73, 79.96, 122.57, 139.69 and 173.29. High resolution mass spectrometry (ESI mass spectrometry [ESI-MS]): calculated for $C_{36}H_{59}O_4$: 555.4413 $[M-H]^+$; found: 555.4465.

Synthesis of (3b)-cholest-5-en-3-yl methyl azelaate (9-CCN-OMe)

Synthesis was performed in the Aldrich MNNG diazomethane generation apparatus according to manufacturer instructions. Briefly, to the outside tube of the apparatus, 2 ml of anhydrous ether and 0.5 ml of chloroform solution of 9-CCN (6 mg/ml, 30.5 mg, 0.06 mmol) was added. The lower part of the assembled apparatus was immersed in the ice and diazomethane was generated by addition of 1 ml of concentrated potassium hydroxide into the inside tube containing a solution of *N*-methyl-*N*-nitroso-p-toluenesulfonamide (0.122 g, 0.57 mmol) in 0.5 ml ethyldiglycol. Apparatus was kept in ice for 2 h and then solvents were evaporated under a gentle stream of nitrogen to give 9-CCN-OMe (33.8 mg, 99%) as a yellowish solid. The crude product was purified by column chromatography on silica gel using dichloromethane as the eluent yielded 32.9 mg (96%) of greater than 99% pure 9-CCN-OMe.

^{1}H-NMR (400 MHz, chloroform-d), δ ppm ^{1}H-NMR 0.69 (s, 3 H), 0.89 (dd, *J* = 6.6, 1.8 Hz, 4 H), 0.94 (d, *J* = 6.6 Hz, 4 H), 1.04 (s, 3 H), 1.17 (m, 6 H), 1.35 (m, 12 H), 1.59 (m, 13 H), 1.87 (m, 2 H), 2.02 (m, 2 H), 2.31 (m, 8 H), 3.69 (s, 3 H), 4.63 (m, 1 H), 5.39 (d, *J* = 4.5 Hz, 1 H); ^{13}C-NMR (100 MHz, chloroform-d), δ ppm 11.84, 18.71, 19.31, 21.02, 22.55, 22.80, 23.82, 24.27, 24.85, 24.83, 24.94, 27.81, 27.99, 28.21, 28.87, 28.93, 31.86, 31.89, 34.03, 34.63, 35.78, 36.18, 36.59, 36.99, 38.15, 39.51, 39.73, 42.30, 50.03, 51.42, 56.13, 56.68, 73.70, 122.58, 139.71 and 173.20. High resolution mass spectrometry (ESI-MS): calculated for $C_{37}H_{64}O_4$: 572.4805 $[M+H]^+$; found: 572.4824.

Synthesis of 9-(cholest-5-en-3-yloxy)-9-oxononanoic acid-d7 (9-CCN-d7)

9-CCN-d_7 was synthesized as described previously for the nondeuterated analogous using 10 mg of cholesterol-d_7 as a precursor. The product was purified by thin-layer chromatography followed by preparative HPLC to give 5 mg (36%) of greater than 99% pure 9-CCN-d_7.

^{1}H-NMR (400 MHz, chloroform-d), δ ppm 0.69 (s, 3 H), 0.90 (d, J = 6.6 Hz, 4 H), 1.00 (d, J = 4.3 Hz, 4 H), 1.11 (m, 10 H), 1.32 (m, 10 H), 1.54 (m, 15 H), 1.83 (m, 4 H), 1.98 (m, 3 H), 2.29 (m, 7 H), 3.52 (m, 1 H), 3.66 (s, 1 H), 4.60 (m, 1 H), 5.35 (m, 1 H); ^{13}C-NMR (100 MHz, chloroform-d), δ ppm 11.85, 18.71, 19.39, 21.08, 23.78, 24.29, 24.60, 24.94, 27.81, 28.22, 28.84, 28.89, 31.65, 31.91, 33.67, 34.31, 35.79, 36.20, 36.51, 36.60, 37.25, 39.27, 39.79, 42.32, 50.14, 56.17, 71.84, 73.74, 117.17, 121.73 and 173.23. High resolution mass spectrometry (ESI-MS): calculated for $C_{36}H_{53}D_7O_4$: 581.5275 $[M+NH_4]^+$; found: 581.5275.

Synthesis of liposomes

Liposomes were prepared by mixing lipid solutions in chloroform in molar ratios as indicated in Table 1. Solvent was evaporated *in vacuo* and the obtained lipid film was hydrated with 20 mM HEPES buffered saline (pH = 7.35; 140 mM NaCl). Next, liposomal suspension was sonicated with probe-type sonicator (Sonicator 3000, Misonix, Inc. Farmingdale, NY, USA) maintaining mixture in the flow of nitrogen gas and cooling with the ice bath. After vesicles are formed, the pH of obtained liposomes was adjusted to 7.20–7.35 by addition of 0.1 M sodium bicarbonate.

Characterization of liposomes

Physical properties of paramagnetic liposomes (i.e., oxPL, PL and mePL) were characterized with respect to size, lamellarity and longitudinal relaxation properties. Size measurements were performed using dynamic light scattering technique on Nano S Zetasizer system (Malvern Instruments, Worcestershire, UK). In addition, size and lamellarity were confirmed by electron microscopy. Longitudinal relaxivity (r_1) measurements were conducted using a 1.5 T scanner at 25°C (Magnetom, Avanto MRI scanner, Siemens Medical Solutions, Erlangen, Germany). Samples were prepared based on Gd concentrations (as determined by inductively coupled plasma mass spectrometry [ICP-MS], see below) as series of dilutions ranging from 1000 to 100 ppm of Gd. Eppendorf tubes were filled with liposomal samples and placed in a styrene box filled with water. Relaxation curves for T_1 were obtained by 2D imaging with an inversion-recovery turbo spin-echo pulse sequence. The following inversion times were applied: 30, 60, 90, 120, 150, 250, 400, 600, 800, 1200, 1600 and 2000 ms. Relaxation times (r_1) were calculated from each slope of the linear relation between $1/T_1$ and Gd concentration.

Annexin V binding assays

Annexin-V-Biotin (BioVision Inc, USA) was added to streptavidin coated #1 coverslips (Xenopore corp., NJ, USA) and incubated for 10 min at room temperature followed by extensive washing with PBS. Next, 25 μl of vesicle formulations with or without PS was added and incubated for 5 min at room temperature. After five washing steps in PBS, coverslips were mounted on microscope slides and examined under Olympus FV1000 spectral confocal microscope using 100× objective. Quantification of rhodamine fluorescence was performed with ImageJ software (NIH, Bethesda, MD, USA).

Ex vivo Gd release

Cumulative release of Gd from liposomal particles (release of free Gd and Gd-DTPA-SA) was determined by dynamic dialysis. In short, aliquots (50 μl) of liposomal formulations were dialyzed (membrane MW cut-off: 12 kDa) against 50 ml of human plasma (obtained from American Red Cross) at 37°C. Plasma sampling was performed at different time intervals and Gd concentrations were obtained using ICP-MS.

Determination of Gd content in liposomes & plasma samples

Plasma samples were digested in a mixture of 70% perchloric acid and 65% nitric acid at 80°C for 8 h. Digested samples were diluted with deionized water and concentration of Gd was determined using Perkin-Elmer Elan 6100 ICP-MS.

Animals

Watanabe heritable hyperlipidemic rabbits (WHHL; Brown Family Enterprises, LLC, Odenville, AL, USA) were fed regular rabbit diet for 10 months. Animals ranging from 3.2 to 3.5 kg were used in *in vivo* experiments. The Institutional Animal Care and Use Committee (IACUC) at The Ohio State University, UH, USA, approved the experimental animal protocols.

Magnetic resonance imaging

The animals were anesthetized with a subcutaneous injection of xylazine (10 mg/kg) and ketamine (50 mg/kg), and placed into the phased array cardiac coil (Siemens, Erlangen, Germany). MRI was performed on 1.5 T Siemens clinical scanner (Magnetom, Avanto) using a coronal gradient echo, T_1-weighted localizing sequence (repetition time/echo time = 800/1.0; field of view = 94 × 125; matrix = 288 × 384). A total of 30 4-mm-thick axial slices spanning approximately from the iliac bifurcation to the superior pole of the topmost kidney were obtained using a T_1-weighted gradient echo turbo FLASH protocol (repetition time/echo time = 230/5; three averages, slice thickness of 4.0 mm with a 5.2–mm gap between slices and a time of acquisition of ~11 m). After precontrast acquisition, 10 ml of oxPL or PL (0.02 mmol/kg of Gd, 10 mmol/kg of total lipids) were injected through marginal ear vein and flushed with 5 ml of normal saline. Images were acquired immediately after the contrast administration for approximately 1 h using repetitive acquisitions of 6-min duration. MRI scans were repeated 12 and 24 h postcontrast administration time points using a single acquisition.

MR images were analyzed using OsiriX image analysis software (The Osirix Foundation, Geneva, Switzerland). The aortic wall was identified and signal intensities of enhanced regions of interest (ROI) were obtained for three slices at each time point. Blind to histopathological data observer performed all ROI measurements. Signal to noise ratio (SNR) of each ROI was calculated as the average signal intensity divided by the standard deviation of the noise level. Relative enhancement ratios with respect to averaged SNR (RER_{SNR}) were calculated and plotted as a percentage decrease in SNR over the time by the formula: $\% RER_{SNR} = 100 \times (SNR_{post}/SNR_{pre})$. SNR_{pre} was obtained from images acquired before contrast agent administration, while SNR_{post} represents SNRs calculated from images acquired 1, 12 and 24 h postinjection. Series of identified ROIs, which matched to histopathological sections, were used for immunostaining followed by confocal microscopy.

Pharmacokinetics studies

All animals subjected to MRI with contrast agent (oxPL or PL) were examined with respect to pharmacokinetics of injected liposomes. The blood was collected from a catheter placed in the marginal ear vein of rabbits by gentle withdrawal with syringe. Sampling was

performed before administration of paramagnetic liposomes as well as 1, 12 and 24 h after contrast agent injection. The plasma was isolated by centrifugation (1000 g, 10 min) and stored at −80°C until analyzed. Gd concentrations in plasma were determined by ICP-MS. Concentrations of 9-CCN in all plasma samples were analyzed by ESI-MS after separation by reverse-phase HPLC. Deuterated internal standard (9-CCN-d_7) was included at a concentration of 2.5 ppm in all plasma samples. Next, proteins were precipitated by adding three volumes of methanol, and supernatant was collected after centrifugation. Pellet was extracted three times with chloroform/methanol mixture (1:1) and combined extracts were evaporated to dryness under a stream of nitrogen. The residue was reconstituted with 90% methanol by sonication followed by isocratic separation on Ascentis 50 × 2.1 mm, 3 μm C18 HPLC column using 90% methanol with 0.1% ammonium acetate as eluent at 0.3 ml/min flow rate. Liquid chromatography was performed using Shimadzu LC-20AD pump interfaced to a Shimadzu CBM-20A system controller (Shimadzu, Columbia, MD, USA). Effluent was analyzed by Applied Biosystems 3200 QTRAP system (Applied Biosystems, Foster, CA, USA) operated in multiple reactions monitoring-positive ionization mode. Specific monitor Q1/Q3 ion pairs were m/z 574.6→369.6 for 9-CCN and m/z 581.6→376.6 for 9-CCN-d_7. Concentrations of 9-CCN were calculated using Analyst software (version 1.4.2, Applied Biosystems). The percentage of injected liposomes at different time points was calculated as described before and based on the average amount of blood plasma in animals of appropriate weight. Plasma volume was assumed to be 3.3% of rabbit body weight.

Immunohistochemistry & confocal microscopy

Segments of abdominal aorta were embedded in optimal cutting temperature compound (Tissue-Tek, Sakura Finetek USA Inc, Torrance, CA, USA) and then frozen in dry ice. The embedded tissues were sectioned at a thickness of 8 μm and placed into cold ethanol. Air-dried slides were hydrated with PBS and treated with 0.2% TritonX-100 in PBS for 2 min. After subsequent washing with PBS and blocking in 1.5% horse serum for 20 min, the slides were stained with RAM-11 primary antibody specific to rabbit macrophages (mouse antirabbit, DAKO, Carpinteria, CA, USA; dilution 1:75) overnight at 4°C. Next, slides were incubated with fluorescently labeled secondary antibody (Cy-5 conjugated goat anti-mouse, Jackson Immuno-Research, West Grove, PA, USA; dilution 1:200) for 90 min at 25°C followed by nuclei staining with Hoescht 33342 (Invitrogen, Carlsbad, CA, USA; dilution 1:1500) for 10 min. Slides were mounted and examined with Zeiss LSM 510 confocal microscope equipped with Argon (458, 477, 488 and 514 nm), green HeNe (543 nm) and red HeNe (633 nm) lasers. For Hoechst 33342 fluorescence Titanium Sapphire two-photon laser was used.

Purification, culture & uptake studies in macrophages derived from peripheral blood monocytes

Monocytes were isolated from buffy coats obtained from the American Red Cross using Ficoll-Hypaque. The cells were further purified using magnetic cell isolation system and CD14 microbeads (Miltenyi Biotec, Auburn, CA, USA). After isolation, monocytes were resuspended in RPMI 1640 medium supplemented with 10% fetal bovine serum (heat inactivated) and seeded in six-well plates. After 2 h, the nonadherent cells were removed and cells were washed with warm medium. The cells were cultured in RPMI supplemented with 10% fetal bovine serum, 1% PSA (penicillin G sodium, streptomycin sulfate and amphotericin B), 10 μg/ml of polymyxin B and 20 ng/ml of M-CSF for 5 days in 37°C with 5% CO_2. The differentiated macrophages were serum-starved for 1 day at 37°C prior to use.

Cells were treated with oxPL or PL formulations and incubated for 30–120 min. Labeled cells were washed, detached and analyzed by flow cytometry using FL2 rhodamine channel

(Accuri Cytometers, Ann Arbor, MI, USA). The capacity of macrophages to ingest oxPL in the presence of a number of antibodies was determined after 1 h of incubation and all data were normalized to control PL uptake values that were obtained in the absence of antibodies. The macrophages were pretreated with anti-$\alpha_v\beta_3$, -$\alpha_v\beta_5$, -CD36 or -scavenger receptor type-1 antibody (all from Millipore, Billerica, MA, USA) for 1 h. The control group was treated with matching isotype (IgG1) antibody.

Lipoproteins

Human low-density lipoprotein (LDL) was isolated from plasma by density ultracentrifugation [17]. Its binding to vesicles was analyzed after separation of vesicle–lipoprotein mixture by ultracentrifugation followed by Lowry protein assay of the vesicle fraction.

Tissue/cell processing & microscopy—Abdominal aorta was sectioned, fixed and stained using previously described methods [18–20]. Cells were grown in glass bottomed dishes (MatTek, Ashland, MA, USA) and treated with BODIPY-LDL or DiI-acLDL (Invitrogen, Carlsbad, CA, USA) with and without vesicles. Confocal fluorescence was performed on a Zeiss LSM 510 microscope.

Results

Vesicle synthesis, physicochemical characterization & *in vitro* testing

Cholesteryl-9-carboxynonanoate was synthesized through a one-step procedure from commercially available azelaic acid and cholesterol (Supplementary Methods & Supplementary Figures 1–4, see online www.futuremedicine.com/doi/suppl/10.2217/nnm.10.87). Lipids were mixed in proportions indicated in Table 1. All vesicles contained equal amounts of Gd-DTPA-SA (paramagnetic lipid) [21] and 0.2% of rhodamine lipid. All vesicle formulations were prepared by means of high-power probe sonication that is known to yield vesicles of uniform size [22]. In addition, vesicle suspensions were passed through 0.2 μm polycarbonate filters in order to remove metal tip particulates and obtain sterile material. Particle size was characterized by dynamic light scattering and TEM. The results show unilamellar vesicles of less than 150 nm in diameter (Figure 2a & Table 1). There were no specific structural differences between vesicles; however, there was a marked increase in polydispersity indices for PL and mePL (Table 1). The incorporation of 9-CCN did not affect vesicle morphology, nor did it alter $1/T_1$ relaxation times in MRI (Figure 2b). Relaxivity values (r_1) for both formulations indicated an approximately twofold increase when compared with commercially used Gd-DTPA (Table 1).

In order to evaluate the stability of prepared vesicles in the *in vivo* context, we examined the capacity of oxPL versus PL to release Gd when exposed to human plasma. This experiment was intended to mimic the physiological context of plasma residence and allowed us to explore potential decomposition of vesicles and subsequent Gd release, which may be important for *in vivo* stability. The vesicles were incubated with human plasma at 37°C and cumulative Gd release was studied using a combination of dynamic dialysis and ICP-MS. The results (Figure 2C) demonstrated that within the first 4 h of dialysis, ≈5% of Gd was released from PL while less than 0.5% of Gd release from the oxPL preparation was noted. During the next approximately 45 h, PL particles released more than 10% of Gd as compared with less than 5% with oxPL. We incubated oxPL, PL and mePL with LDL for 1 h and compared electrophoretic mobilities of resulting protein–lipid adducts with that of unmodified LDL (Figure 2d). LDL but not phospholipid vesicles were detectable on the gel (due to excess LDL [1 μg LDL/100 μg of vesicle lipids] and inability of vesicles to migrate

owing to size restrictions) (Figure 2d). Incubation with oxPL vesicles (lane 2) gave rise to two bands, one corresponding to a highly electronegative band (arrow) and another band with slower mobility (arrowhead, Figure 2d). The highly mobile band most likely represents lipids inherent in vesicles bound to LDL. This component might account for the accelerated and enhanced uptake by macrophages. The lower band with slower mobility across the electrochemical gradient may represent the dominant LDL component with a low concentration of vesicle lipids, rendering a small but discernible shift in electrophoretic mobility of LDL. This band perhaps reflects the component with longer plasma half-life. Consistent with this, the band intensity of the LDL particles treated with oxPL was less compared with the intensities of PL- and mePL-treated LDL, suggesting a greater affinity of LDL for the oxPL liposomal formulation. Methylation of the 9-CCN resulted in the abolition of the changes in mobility seen on incubation of oxPL with LDL, confirming the need for the ω-carboxylic group in electrostatic interactions. Incubation of vesicles with fresh LDL followed by ultracentrifugation and quantification of protein content confirmed significant preferential binding of LDL to oxPL as compared with PL vesicles (Figure 2e). Figure 2F depicts TEM images of the oxPL in the presence of LDL. In contrast to the morphology of vesicles not incubated with LDL (not shown), the new particles demonstrated discrete disk-like structures embedded in a matrix surrounding the vesicle core. The size of the disks approximately corresponded to the size of LDL particles (20 nm) [23].

Estimation of thermal stability of formulations was carried out under heat sterilization conditions followed by exhaustive dialysis. Gd loss from vesicles was quantified by ICP-MS. We used micellar preparations as a representative control as these have been used recently as part of various targeted MRI-based strategies [2, 7]. Figure 2g depicts gross visual aggregation of the micellar particles, while oxPL and PL visually appeared to be homogeneous, oxPL showed superior heat resistance with minimal particle aggregation and Gd loss (Figure 2h & 2i).

In order to evaluate the presence of PS on the outer membrane of the particles, Annexin V coverslips were treated with rhodamine-containing oxPL and PL formulations (prepared with and without PS). After several washing steps with PBS, coverslips were mounted on microscope slides and examined under a confocal microscope (Figure 3a). Vesicles containing PS were detected on coverslips by intrinsic rhodamine fluorescence as numerous bright dots. At the same time formulations without PS showed no or little rhodamine fluorescence (Figure 3b). Quantification of rhodamine-positive particles was performed with ImageJ software (Figure 3C). The results show that vesicles containing PS readily form a stable Annexin V complex on the surface of the coverslip.

In order to demonstrate that oxPL vesicles exhibit synthetic oxidized cholesterol ester (9-CCN) on their outer surface, we analyzed different formulations with respect to their zeta potential (Table 1). oxPL particles demonstrated the highest zeta potential (−69.95 mV), suggesting that carboxyl groups present on the surface of the particles significantly contribute to the overall negative charge. By contrast, when a methylated derivative of 9-CCN was used for vesicle preparation (mePL vesicles), the zeta-potential value was determined to be very close to that for PL vesicles (−45.21 and −46.92, respectively), indicating the abolished effect of the ‘naked’ carboxyl group.

N-acetyl derivatives of PS are known to induce thrombosis [24], while numerous *in vitro* and *in vivo* studies suggest that PS itself is not active in platelet aggregation [25, 26]; nevertheless, we tested whether oxPL could induce platelet aggregation *in vitro.* Platelets were isolated from the blood of a healthy donor and resuspended in calcium-containing buffer. Control (PBS), oxPL vesicles or thrombin were added and platelet aggregation was

monitored with the aggregometer. We could not detect an increased platelet aggregation with oxPL (data not shown). The results provide additional support for the safety of oxPL use *in vivo*.

In vivo MRI & pharmacokinetics assessment

We performed *in vivo* validation in the WHHL model on a 1.5 T clinical scanner. Rabbits were injected with either oxPL or PL (0.02 mmol/kg of Gd). Uptake of vesicles in the abdominal aorta was observed at 1, 12 and 24 h postinjection. These timings were chosen to represent several fold higher potential $T_{1/2}$ of the particles. Delineation of vessel wall was seen even at 24 h postcontrast injection with oxPL, but not with PL (Figure 4a). We are able to discriminate lumen from the wall very clearly in light of the fact that we use a superior flow-saturation pulse to void luminal signal in the aorta. The areas of uptake corresponded to plaque (Supplementary Figure 5). Relative enhancement ratios (RER_{SNR}) were calculated at 0.2, 0.4, 0.6, 0.8, 1, 12 and 24 h and used as semiquantitative measures of plaque enhancement over time (details on image analysis can be found in Supplementary in Formation). Figure 4b depicts contrast enhancement of aorta over time and indicates persistent signal with oxPL up to 24 h. Pharmacokinetics of the preparations were assessed by quantification of Gd in blood collected at the same time points as the MRI and revealed detectable Gd in the oxPL at 24 h but not the PL vesicle group (Figure 4C). Additional confirmation of prolonged plasma kinetics of 9-CCN vesicles was obtained by quantification of 9-CCN in plasma using MS (Supplementary methods & Supplementary Figure 6). The analysis of SNR in the inferior vena cava, kidney and muscle demonstrated that the evolution of SNR in these organs is distinctly different than the aortic wall (Figure 4d & 4e).

Colocalization of oxPL with plaque macrophages

Figure 5 demonstrates characteristic rhodamine fluorescence in abdominal aortic sections from the animals that received oxPL but not in the animals receiving PL. Merge images show colocalization of oxPL in macrophage containing loci. Macrophages were detected diffusely in both oxPL and PL groups, depicted in Figure 5 as green staining (Cy-5 dye, green pseudo color).

In vitro studies of uptake & phagocytosis pathways of anionic vesicles

Human macrophages were incubated with vesicles or controls for 120 min. Followed by assessment of rhodamine content in the incubated cells. Figure 6a shows rapid uptake of oxPL compared with PL binding resulting in approximately five-fold increase in uptake after 2 h of incubation. Interestingly, the uptake of oxPL as compared with vesicles containing methyl ester modified 9-CCN (mePL) was significantly lower, suggesting an effect of the ω-carboxylic group in oxPL in mediating uptake (Figure 6b). To further understand the mechanisms of uptake of oxPL vesicles we performed incubation experiments in cultured human macrophages. In these experiments oxPL or PL at various concentrations was incubated with labeled LDL for 1 h, followed by treatment of macrophages for a duration of 15 min. The fluorescence intensity of BODIPY-LDL was quantified and expressed as a function of vesicle lipid concentrations. Figure 7a depicts higher uptake of labeled LDL in the presence of oxPL. Figure 7b depicts representative confocal microscopic images of cells incubated with oxPL in the presence of LDL and demonstrates increased uptake of both LDL and oxPL. In comparison, incubation of LDL with PL had a weaker effect in mediating LDL uptake as well as the uptake of PL vesicles (Figure 7C). Performance of the same experiment at 4°C markedly attenuated uptake, implicating a receptor-dependent mechanism of uptake [27]. We repeated the incubation experiments with labeled acetyl LDL, which is highly negatively charged. The uptake of oxPL and PL was nearly identical in the presence of acetyl LDL, suggesting that positively charged residues (e.g., lysine residues that are well known to be abundant in LDL) is a

requirement for uptake of oxPL (Figure 7d). To study possible uptake pathway(s), we performed experiments where macrophage engulfment was blocked by the antibodies against receptor pathways commonly implicated in the process of macrophage engulfment (Figure 7e). The cells were incubated with different antibodies or control isotype IgG followed by incubation with oxPL or PL. The uptake was assessed by flow cytometry. The inhibition of the integrin receptor $\alpha_v\beta_3$ showed maximal reduction in the uptake of oxPL, followed by the antibodies targeting $\alpha_v\beta_5$. Scavenger receptor A (SR-A) reduced the uptake, but not significantly ($p = 0.09$). Since the cellular responses of macrophages vary considerably depending on context (engulfment of pathogens/foreign substances vs engulfment of apoptotic debris) we tested TNF-α release 2 h following uptake of vesicles. TNF-α release by macrophages was lower in the oxPL group as compared with the PL ingested vesicles, suggesting the attenuation of inflammatory effects by 9-CCN oxidized lipids (Figure 7F).

Discussion

In this study we tested the ability of paramagnetic anionic vesicle probes incorporating specific oxidatively modified lipids to detect macrophages in a large animal model of atherosclerosis. Our approach relied on the well-known ability of macrophages to engulf oxidatively modified lipoproteins and apoptotic cell membranes containing anionic phospholipids, such as PS [28]. The preferential uptake of synthetic paramagnetic vesicles containing both PS and oxidatively modified lipids resulted in enhancement of atherosclerotic lesions rich in macrophages by MRI. The exposure of PS, normally found in the inner leaflet of the plasma membrane, is probably the best-studied ‘eat-me’ signal and either directly (naked PS) or in conjunction with other bridging molecules, such as MFGE8, annexin V may facilitate macrophage engulfment [8]. No single PS-specific receptor appears to be involved and instead a wide variety of macrophage cell-surface receptors have been implicated in PS recognition, including SR-A, CD36, receptors that recognize bridging molecules, and integrin receptors, suggesting that the recognition may be entirely context dependent [8]. Additional theoretical advantages of using PS-containing vesicles include their anti-inflammatory effects on macrophages, resulting in production of TGF-β and PPAR-γ activation [10, 29]. In this study, we hypothesized that incorporation of oxidized analogs of cholesterol (9-CCN) may serve as an additional ligand for macrophage uptake and may be superior to PS-containing vesicles alone.

Physicochemical characterization of PS vesicles additionally modified with 9-CCN (oxPL) showed round structures of uniform size. The presence of 9-CCN decreased oxPL vesicle lamellarity as compared with other formulations and evidenced by polydispersity indices (Table 1). The increased zeta potential of oxPL suggested that carboxylic residues of 9-CCN are expressed on the surface of particles.

Our *in vitro* characterization work suggested that the oxPL preparation did not undergo changes in size even after prolonged incubation in human plasma and released minimal amounts of Gd (<5% over 48 h). Moreover, the incorporation of 9-CCN significantly improved the stability of the vesicles even under ‘autoclave’ conditions. This is an important attribute that would theoretically allow the preparation to be scaled up for human use in potential ‘theranostic’ applications that combine molecular imaging with local therapy [30].

Our results seem to suggest binding of LDL to the 9-CCN containing oxPL vesicles. This is evidenced in our *in vitro* coincubation experiments by a distinct band on electrophoresis, altered migration properties of LDL, characteristic effects on liposome morphology and quantification of oxPL bound to LDL. *In vitro* uptake of our probe using cultured human macrophages demonstrated rapid uptake of oxPL compared with PL, resulting in

approximately fivefold increase in uptake after 2 h of incubation and suggests involvement of a highly efficient uptake pathway, such as the scavenger receptor pathway. The presence of the ω-carboxylic group in oxPL was essential in mediating preferential uptake, as evidenced by abrogation of uptake by methylation of the carboxylic acid at this position. This is consistent with prior studies that have demonstrated an essential role for this group in uptake of vesicles containing 7-ketocholesteryl-13-carboxytridecanoate by murine J774A.1 cells [31, 32]. In addition, our vesicles exerted anti-inflammatory effects by lowering TNF-α levels. This property of 'passivation' of macrophages may have important ramifications for proinflammatory diseases.

The binding of LDL to oxPL particles may have additional implications for targeted imaging as modified forms of oxidatively modified forms of LDL are rapidly taken up by highly efficient scavenger receptor pathways. Indeed, prior studies have suggested that LDL may directly interact with anionic nanoparticles [33] and liposomes [34], promoting their uptake by the macrophages. Our experiments showing enhanced uptake of oxPL in the presence of LDL, but not acetyl LDL, implicate a charge-based interaction between LDL and oxPL that may then modulate uptake by the macrophage. Additional experiments performed with specific antibodies suggest a role for integrin pathways. These experiments are meant to be interpreted together and are not mutually exclusive. It is possible that the antibodies used in the study are not 'blocking' antibodies and may not reflect the contribution of various scavenger receptor pathways. It is also possible that 9-CCN (which has not been tested) may have interacted with other receptor pathways, including those responsible for the uptake of apoptotic cells, such as MFG-E8 [35].

In vivo studies in the WHHL model confirmed delayed enhancement of plaque with colocalization in macrophage-rich areas. A deliberate aspect of this study was the employment of a large animal model that would recapitulate abnormalities in LDL metabolism while at the same time facilitates imaging at clinically relevant field strengths. The WHHL model is typified by absent LDL receptors, LDL cholesterol levels greater than 750 mg/dl [36] and accelerated atherosclerosis. The increase in signal intensity in the abdominal aorta was maintained at the last tested time point of 24 h. At the same time we observed protracted venous signal, probably due to artifacts inherent for imaging protocol used (gradient echo sequence with FLASH™). In this case the signal is related to unsaturated blood that enters the slices in the opposite direction of the aortic blood and is consequently not subject to a flow-saturation pulse to which the aortic blood is subjected. However, the presence of contrast in the venous circulation may enhance T_1 relaxivity and may contribute to higher signal postcontrast.

Increased availability of the contrast probe in the intravascular compartment was confirmed by higher levels of Gd (analyzed with ICP-MS) and 9-CCN content (quantified with ESI-MS). Our results demonstrate that the oxPL agent has a longer circulation half-life than the control. We cannot exclude the possibility that the greater contrast enhancement observed for the oxPL agent is not only due to specific macrophage binding but also potentially due to that longer half-life. Unfortunately, we could not determine exact half-life values for oxPL or PL due to a limited number of animals that were available for this study. In Figure 3, with 25% of the oxPL dose remaining in the serum at 24 h, it seems reasonable to suggest that the half-life of oxPL is approximately 12 h. In comparison, the control particle has a much shorter half-life, perhaps 3–4 h.

The experiments in Figure 7 were meant to address specific charge interactions between our preparation and common lipoprotein moieties that may have implications for clearance/retention. It is well known that LDL is the dominant lipoprotein species in humans and in the WHHL rabbit model used in this work. The major fraction of LDL is characterized by

electropositive charge due to exposed lysine residues of apoB-100 [37]. In response to oxidative modifications to the apoB-100 and cholesterol components, oxidized modifications of LDL are profoundly negatively charged and are rapidly cleared by scavenger receptor pathways [38]. Oxidized or acetylated LDLs are rapidly cleared by the liver in mice with disruption of the scavenger receptor class A type I/II gene [38, 39]. Highly negatively charged LDL species, such as acetyl LDL and oxidized LDL, have a plasma half-life of less than 10 min. The extent of oxidation or acetylation is therefore an important determinant of clearance rate. The fact that the liposomes employed in our experiments contained oxidized lipids (i.e., strongly negatively charged) would imply rapid clearance from the circulation, yet our data seemed to suggest otherwise. Therefore, we posited that the interaction of our preparation with LDL in the plasma may result in important modifications in the charge of the collective entity. Thus, while the free negatively charged liposomes might be cleared rapidly by the reticuloendothelial system, particles that are bound or associated with LDL might have a longer circulatory dwell time.

Figure 7 examined the uptake of fluorescently labeled LDL in the presence of oxPL and PL. The results clearly show that in the presence of LDL there is higher degree of uptake of oxPL compared with the PL (Figure 7a). A representative experiment is depicted in Figure 7b (oxPL with LDL) and Figure 7C (PL with LDL); the uptake is receptor dependent (abolished at 4°C compared with 37°C; Figure 7b & 7C); charge is a major determinant of uptake (Figure 7d).

We did not perform organ-specific biodistribution studies to answer the question on accumulation vesicles. According to the literature, liposomes and other lipid vesicles tend to accumulate in liver, spleen and kidney (reticulo-endothelial system) [40]. Analysis of MRI images (Figure 4d & 4e) indicates increased contrast in kidneys 24 h after injection while showing no altered enhancement in muscle for both tested vesicle formulations. These results allow us to speculate that a large fraction of contrast material accumulated after 24 h is not in the muscle but in organs of the reticuloendothelial system.

Our approach represents an alternative to other delivery platforms, including micelles and immunoliposomes, that have also been used to image macrophages in tumors and atherosclerosis. A promising nanoparticle platform to deliver MR contrast agents consists of amphiphilic phospholipids that self-assemble into micelles or liposomes. The incorporation of paramagnetic/supermagnetic reporters (Gd- or Fe-oxide-based) into antibody-conjugated preparations may confer selectivity and discrimination. Numerous studies have shown that when delivered as immunomicelles [2, 3] or liposomes [41–43], these agents recognize specific epitopes or cell populations and selectively accumulate in pathological sites enabling detection. The additional conjugation to therapeutic agents imparts the potential for intervening and simultaneously assessing response to treatment [44, 45].

One of the limitations of our study is the use of antibodies to assess uptake pathways and make conclusions regarding the precise receptors that may be involved in the engagement and eventual engulfment of our preparations. The absence of significant effects in preventing uptake of our preparations in cultured macrophages may still not preclude an important role for CD36 or SR-A receptors. In fact, CD36-/SR-A-dependent mechanisms have been shown previously to be of importance in the recognition and disposition of PS and oxidized lipids in apoptotic cell debris [8]. An additional limitation is the precise intracellular localization of our vesicles once taken up by the macrophage. An important implication of our studies is the ready translatability of these results to the imaging of macrophages in atherosclerosis and cancer.

Conclusion

In conclusion, we have provided initial proof-of-concept studies for a novel probe incorporating oxidatively tailored lipids to target and image macrophages. Our demonstration of feasibility at a clinically relevant field strength, use of small quantities of paramagnetic contrast agent, stability of the preparation and ability to scale-up synthesis are key strengths that may allow extension of such an approach for clinical imaging of atherosclerosis.

Future perspective

The availability of tailored contrast agents that allow noninvasive detection of inflammation within atherosclerotic plaque by MRI will enable pre-emptive detection of 'high-risk' patients. This will then facilitate therapeutic intervention to prevent future cardiovascular events.

Supplementary Material

Refer to Web version on PubMed Central for supplementary material.

Acknowledgments

The authors would like to thank Jeffrey Deiuliis for insightful comments and remarks on the manuscript.

Bibliography

Papers of special note have been highlighted as:

▪ of interest

▪▪ of considerable interest

1▪. Cormode DP, Skajaa T, Fayad ZA, Mulder WJ. Nanotechnology in medical imaging: probe design and applications. Arterioscler Thromb Vasc Biol. 2009; 29(7):992–1000. A concise, yet comprehensive review that describes different nanoplatforms used for atherosclerosis imaging. [PubMed: 19057023]

2▪▪ . Amirbekian V, Lipinski MJ, Briley-Saebo KC, et al. Detecting and assessing macrophages *in vivo* to evaluate atherosclerosis noninvasively using molecular MRI. Proc Natl Acad Sci USA. 2007; 104(3):961–966. Important paper outlining a gadolinium micelle-based strategy to selectively image macrophages in a mouse model of atherosclerosis using high-field (9.4 T) MRI. [PubMed: 17215360]

3▪▪ . Briley-Saebo KC, Shaw PX, Mulder WJ, et al. Targeted molecular probes for imaging atherosclerotic lesions with magnetic resonance using antibodies that recognize oxidation-specific epitopes. Circulation. 2008; 117(25):3206–3215. Elegant work introducing the applicability of novel micellar contrast agents targeted to atherosclerosis by means of micelle-coupled antibodies against oxidized low-density lipoprotein. [PubMed: 18541740]

4. Chen W, Vucic E, Leupold E, et al. Incorporation of an apoE-derived lipopeptide in high-density lipoprotein MRI contrast agents for enhanced imaging of macrophages in atherosclerosis. Contrast Media Mol Imaging. 2008; 3(6):233–242. [PubMed: 19072768]

5▪ . Frias JC, Williams KJ, Fisher EA, Fayad ZA. Recombinant HDL-like nanoparticles: a specific contrast agent for MRI of atherosclerotic plaques. Am Chem Soc. 2004; 126(50):16316–16317. Landmark paper describing how natural high-density lipoprotein nanoparticles can be utilized as targeted to atherosclerosis imaging probes.

6. Bruns OT, Ittrich H, Peldschus K, et al. Real-time magnetic resonance imaging and quantification of lipoprotein metabolism *in vivo* using nanocrystals. Nat Nanotechnol. 2009; 4(3):193–201. [PubMed: 19265850]

7. Peters D, Kastantin M, Kotamraju VR, et al. Targeting atherosclerosis by using modular, multifunctional micelles. Proc Natl Acad Sci USA. 2009; 106(24):9815–9819. [PubMed: 19487682]

8▪▪ . Ravichandran KS, Lorenz U. Engulfment of apoptotic cells: signals for a good meal. Nat Rev Immunol. 2007; 7(12):964–974. Comprehensive review paper outlining a variety of important moleclular signals responsible for apoptotic cell recognition. [PubMed: 18037898]

9▪▪ . Greenberg ME, Li XM, Gugiu BG, et al. The lipid whisker model of the structure of oxidized cell membranes. Biol Chem. 2008; 283(4):2385–2396. State-of-the-art research work introducing the conceptual model of the distribution of oxidized phospholipid moieties on the outer membrane leaflet. This paper is one in a series of recent publications on the investigation of oxidized lipids and phosphatidylserine in cellular recognition (also see other works by SL Hazen).

10▪ . Huynh, Ml; Fadok, VA.; Henson, PM. Phosphatidylserine-dependent ingestion of apoptotic cells promotes TGF-β1 secretion and the resolution of inflammation. Clin Invest. 2002; 109(1):41–50. Demonstrates that macrophage engulfment of cellular apoptotic debris containing membrane phosphatidylserine is prone to reduce inflammatory response.

11. Steinberg D, Parthasarathy S, Carew TE, Khoo JC, Witztum Jl. Beyond cholesterol. Modifications of low-density lipoprotein that increase its atherogenicity. N Engl Med. 1989; 320(14):915–924.

12. Fossheim, Sl; Fahlvik, AK.; Klaveness, J.; Muller, RN. Paramagnetic liposomes as MRI contrast agents: influence of liposomal physicochemical properties on the *in vitro* relaxivity. Magn Reson Imaging. 1999; 17(1):83–89. [PubMed: 9888401]

13. Kritharides L, Jessup W, Gifford J, Dean RT. A method for defining the stages of low-density lipoprotein oxidation by the separation of cholesterol- and cholesteryl ester-oxidation products using HPLC. Anal Biochem. 1993; 213(1):79–89. [PubMed: 8238886]

14. Campos SM, Penson RT, Mays AR, et al. The clinical utility of liposomal doxorubicin in recurrent ovarian cancer. Gynecol Oncol. 2001; 81(2):206–212. [PubMed: 11330951]

15. Al-Batran SE, Bischoff J, Von Minckwitz G, et al. The clinical benefit of PEGylated liposomal doxorubicin in patients with metastatic breast cancer previously treated with conventional anthracyclines: a multicentre Phase II trial. Br Cancer. 2006; 94(11):1615–1620.

16. Parac-Vogt TN, Kimpe K, Laurent S, et al. Paramagnetic liposomes containing amphiphilic bisamide derivatives of Gd-DTPA with aromatic side chain groups as possible contrast agents for magnetic resonance imaging. Eur Biophys J. 2006; 35(2):136–144. [PubMed: 16217648]

17. Havel RJ, Eder HA, Bragdon JH. The distribution and chemical composition of ultracentrifugally separated lipoproteins in human serum. Clin Invest. 1955; 34(9):1345–1353.

18. Rajagopalan S, Duquaine D, King S, Pitt B, Patel P. Mineralocorticoid receptor antagonism in experimental atherosclerosis. Circulation. 2002; 105(18):2212–2216. [PubMed: 11994257]

19. Sirol M, Itskovich VV, Mani V, et al. Lipid-rich atherosclerotic plaques detected by gadofluorine-enhanced *in vivo* magnetic resonance imaging. Circulation. 2004; 109(23):2890–2896. [PubMed: 15184290]

20. Hyafil F, Laissy JP, Mazighi M, et al. Ferumoxtran-10-enhanced MRI of the hypercholesterolemic rabbit aorta: relationship between signal loss and macrophage infiltration. Arterioscler Thromb Vasc Biol. 2006; 26(1):176–181. [PubMed: 16269663]

21. Montembault V, Soutif JC, Brosse JC. Synthesis of chelating molecules as agents for magnetic resonance imaging. 3. Polycondensation of diethylenetriaminepentaacetic acid bisanhydride with diols and diamines. React Funct Polym. 1996; 29(1):29–39.

22. Papahadjopoulos D, Watkins JC. Phospholipid model membranes. II. Permeability properties of hydrated liquid crystals. Biochim Biophys Acta. 1967; 135(4):639–652. [PubMed: 6048247]

23. Forte TM, Carlson LA. Electron microscopic structure of serum lipoproteins from patients with fish eye disease. Arteriosclerosis. 1984; 4(2):130–137. [PubMed: 6704050]

24. Martin TW, Joist JH, Bauman JE, Lagunoff D. Activation of human platelets by *N*-substituted aminophospholipids. Biol Chem. 1985; 260(5):2852–2856.

25. Mustard JF, Medway W, Downie HG, Rowsell HC. Effects of intravenous phospholipid containing phosphatidyl serine on blood clotting with particular reference to the Russell's viper venom time. Nature. 1962; 196:1063–1065. [PubMed: 13936889]
26. Brunauer LS, Huestis WH. Effects of exogenous phospholipids on platelet activation. Biochim Biophys Acta. 1993; 1152(1):109–118. [PubMed: 8399288]
27. Goldstein JL, Ho YK, Basu SK, Brown MS. Binding site on macrophages that mediates uptake and degradation of acetylated low density lipoprotein, producing massive cholesterol deposition. Proc Natl Acad Sci USA. 1979; 76(1):333–337. [PubMed: 218198]
28. Libby P. Inflammation in atherosclerosis. Nature. 2002; 420(6917):868–874. [PubMed: 12490960]
29. Ramos GC, Fernandes D, Charao CT, Souza DG, Teixeira MM, Assreuy J. Apoptotic mimicry: phosphatidylserine liposomes reduce inflammation through activation of peroxisome proliferator-activated receptors (PPARS) *in vivo*. Br Pharmacol. 2007; 151(6):844–850.
30. Jaffer, Fa; Libby, P.; Weissleder, R. Optical and multimodality molecular imaging: insights into atherosclerosis. Arterioscler Thromb Vasc Biol. 2009; 29(7):1017–1024. [PubMed: 19359659]
31. Kobayashi K, Matsuura E, Liu Q, et al. A specific ligand for β(2)-glycoprotein I mediates autoantibody-dependent uptake of oxidized low density lipoprotein by macrophages. Lipid Res. 2001; 42(5):697–709.
32. Liu Q, Kobayashi K, Furukawa J, et al. Omega-carboxyl variants of 7-ketocholesteryl esters are ligands for β(2)-glycoprotein I and mediate antibody-dependent uptake of oxidized LDL by macrophages. Lipid Res. 2002; 43(9):1486–1495.
33▪. Chnari E, Lari HB, Tian L, Uhrich KE, Moghe PV. Nanoscale anionic macromolecules for selective retention of low-density lipoproteins. Biomaterials. 2005; 26(17):3749–3758. Describes an interesting observation that anionic nanoparticles can associate with natural low-density lipoprotein. [PubMed: 15621265]
34. Greenspan P, Ryu BH, Mao F, Gutman RL. Association of negatively-charged phospholipids with low-density lipoprotein (LDL) increases its uptake and the deposition of cholesteryl esters by macrophages. Biochim Biophys Acta. 1995; 1257(3):257–264. [PubMed: 7647101]
35. Hanayama R, Tanaka M, Miyasaka K, et al. Autoimmune disease and impaired uptake of apoptotic cells in MFG-E8-deficient mice. Science. 2004; 304(5674):1147–1150. [PubMed: 15155946]
36. Yamada N, Shimano H, Mokuno H, et al. Increased clearance of plasma cholesterol after injection of apolipoprotein E into watanabe heritable hyperlipidemic rabbits. Proc Natl Acad Sci USA. 1989; 86(2):665–669. [PubMed: 2911597]
37. Blanco FJ, Villegas S, Benitez S, et al. 2D-NMR reveals different populations of exposed lysine residues in the apoB-100 protein of electronegative and electropositive fractions of LDL particles. Lipid Res. 2010; 51(6):1560–1565.
38. Ling W, Lougheed M, Suzuki H, Buchan A, Kodama T, Steinbrecher UP. Oxidized or acetylated low density lipoproteins are rapidly cleared by the liver in mice with disruption of the scavenger receptor class a type I/II gene. Clin Invest. 1997; 100(2):244–252.
39. Nagelkerke JF, Barto KP, Van Berkel TJ. *In vivo* and *in vitro* uptake and degradation of acetylated low density lipoprotein by rat liver endothelial, kupffer, and parenchymal cells. Biol Chem. 1983; 258(20):12221–12227.
40. Hardy JG, Kellaway IW, Rogers J, Wilson CG. Distribution and fate in the rabbit of liposomes containing [^{131}I]-sodium iodide. Br Pharmacol. 1979; 67(3):459P.
41. Briley-Saebo KC, Mulder WJ, Mani V, et al. Magnetic resonance imaging of vulnerable atherosclerotic plaques: current imaging strategies and molecular imaging probes. Magn Reson Imaging. 2007; 26(3):460–479.
42. Reulen SW, Brusselaars WW, Langereis S, Mulder WJ, Breurken M, Merkx M. Protein–liposome conjugates using cysteine-lipids and native chemical ligation. Bioconjug Chem. 2007; 18(2):590–596. [PubMed: 17315942]
43. Brandwijk RJ, Mulder WJ, Nicolay K, Mayo KH, Thijssen Vl, Griffioen AW. Anginex-conjugated liposomes for targeting of angiogenic endothelial cells. Bioconjug Chem. 2007; 18(3):785–790. [PubMed: 17378601]

44. Wickline SA, Neubauer AM, Winter PM, Caruthers SD, Lanza GM. Molecular imaging and therapy of atherosclerosis with targeted nanoparticles. Magn Reson Imaging. 2007; 25(4):667–680.

45. Kluza E, Van Der Schaft DW, Hautvast PA, et al. Synergistic targeting of integrin $\alpha_V\beta_3$ and galectin-1 with heteromultivalent paramagnetic liposomes for combined MR imaging and treatment of angiogenesis. Nano Lett. 2010; 10(1):52–58. [PubMed: 19968235]

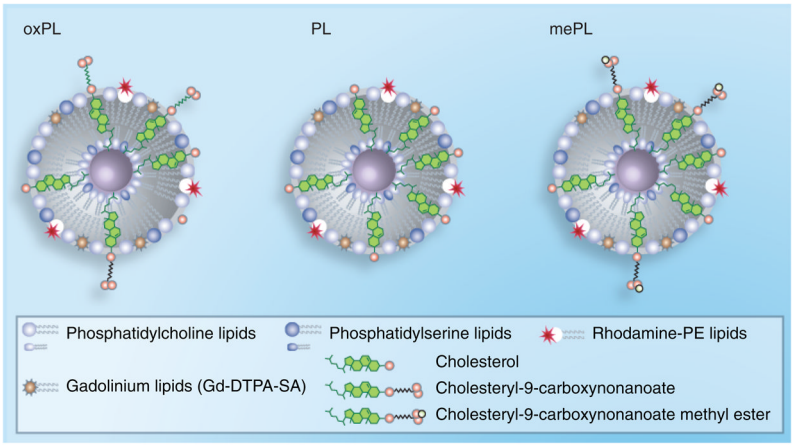

Figure 1. Schematic representation of synthesized vesicles

PL vesicles were generated from commercially available phospholipids and cholesterol. oxPL vesicles were synthesized with cholesteryl-9-carboxynanoate to mimic oxidized phospholipids while providing targeting to macrophages. mePL vesicles were formulated with cholesteryl-9-carboxynanoate methyl ester and served as nontargeted control. All formulations contained Gd lipids and rhodamine for MRI and fluorescence detection in cells and tissues.

Gd: Gadolinium; mePL: (3b)-cholest-5-en-3-yl methyl azelaate phospholipid vesicles; oxPL: Cholesteryl-9-carboxynonanoate phospholipid vesicles; PL: Phospholipid.

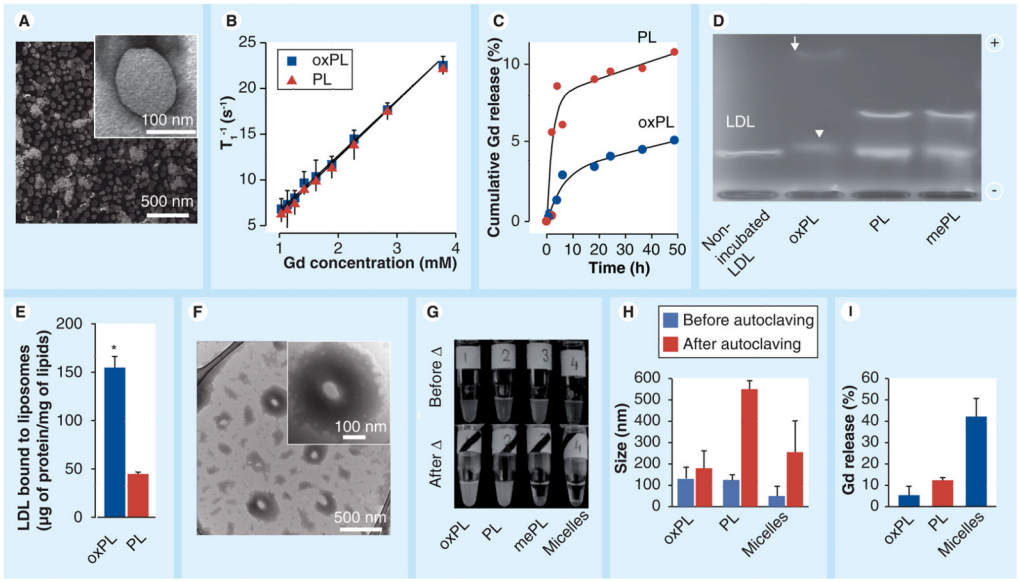

Figure 2. Characterization of vesicles containing 9-CCN (oxPL) and control (PL)

(A) Electron micrographs of oxPL show round unilamellar vesicles approximately 100 nm in diameter (inset). **(B)** relaxivity of oxPL and PL containing different Gd concentrations at T_1 1.5 T. **(C)** *In vitro* Gd release in human plasma as measured by inductively coupled plasma mass spectrometry. **(D)** Agarose electrophoresis of human LDL incubated with vesicle formulations. The arrow indicates a highly mobile electronegative band while the arrow head indicates slightly higher electrophoretic mobility, but with lower densitometric concentration of LDL. **(E)** LDL was incubated with oxPL or PL followed by ultracentrifugation and quantification of LDL protein. **(F)** Vesicles were incubated with LDL followed by transmission electron microscopy. oxPL tends to accumulate LDL lipids on its surface resulting in lipid 'cloud' formation around the core (inset). **(G)** Photographs of vesicle preparations and miceller solutions before and after autoclaving. Moderate aggregation was observed for oxPL while complete water–lipid phase separation was seen for micelles and mePL. **(H)** Particle size by dynamic light scattering before and after autoclaving. **(I)** Following autoclaving all formulations were subjected to exhaustive dialysis and Gd release was determined as a ratio of the final Gd concentrations to the concentrations obtained before experiment. *$p < 0.01$

Gd: Gadolinium; LDL: Low-density lipoprotein; mePL: (3b)-cholest-5-en-3-yl methyl azelaate phospholipid vesicles; oxPL: Cholesteryl-9-carboxynonanoate phospholipid vesicles; PL: Phospholipid.

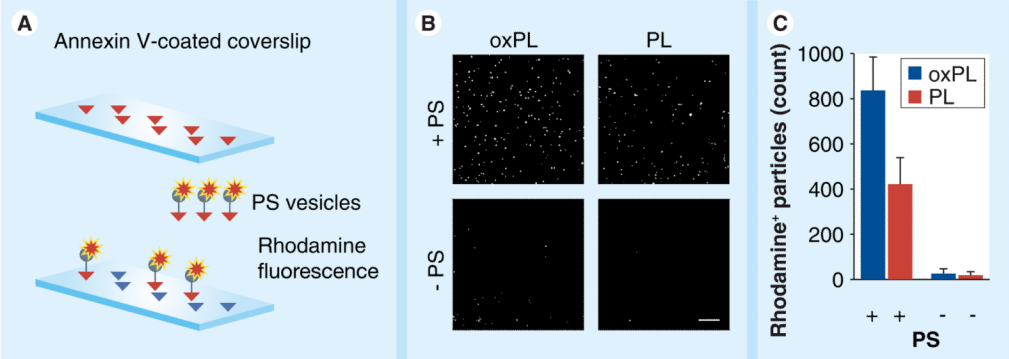

Figure 3. Evaluation of the presence of phosphatidylserine on the outer membrane of the vesicles

(A) Experimental design scheme. Annexin V coverslips were used in order to test whether oxPL or PL exhibit PS on the outer membrane. **(B)** Confocal microscopy images of coverslip areas incubated with vesicles containing PS and those prepared without PS. Bar size is 20 μm. **(C)** Quantification of vesicles bound to coverslip by number of fluorescent particles.

oxPL: Cholesteryl-9-carboxynonanoate phospholipid vesicles; PS: Phosphatidylserine; PL: Phospholipid.

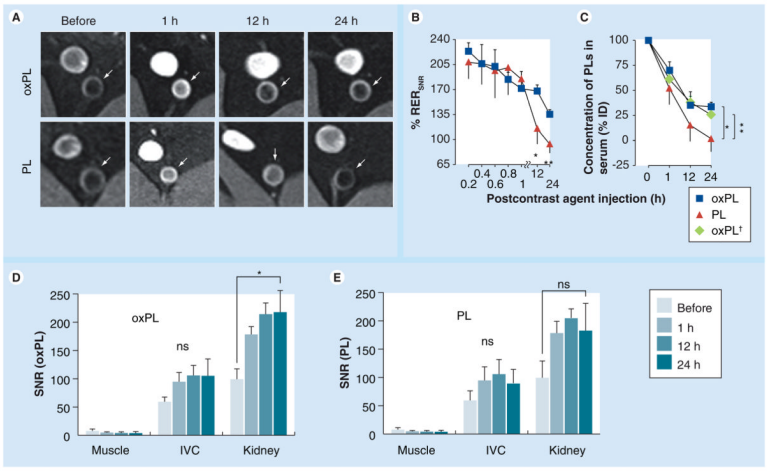

Figure 4. *In vivo* testing of the vesicles

(A) T_1-weighted MR images of atherosclerotic abdominal aorta after oxPL or PL administration. Signal enhancement in plaque (white arrows) was seen over a 24-h period with oxPL but not PL. **(B)** Time course of MR signal enhancement. The difference in enhancement between pre- and post-contrast injection is presented as relative enhancement ratio The amount of gadolinium in serum was quantified over time using inductively coupled plasma mass spectrometry for (RER_{SNR}). **(C)** oxPL- and PL-injected animals (n = 5 and n = 3, respectively). Cholesterol-9-carboxynonanoate concentration in serum was determined by LC-MS for oxPL-injected rabbits (n = 5, $oxPL^{\dagger}$ plot). Concentration of PL in serum is presented as percentage of dose injected. **(D & E)** Analysis of SNR (oxPL and PL, respectively) in the muscle, IVC and kidney. *p < 0.05; **p < 0.001.

IVC: Inferior vena cava; ns: Not significant; oxPL: Cholesteryl-9-carboxynonanoate phospholipid vesicles; PL: Phospholipid; RER: Relative enhancement ratio; SNR: Signal to noise ratio.

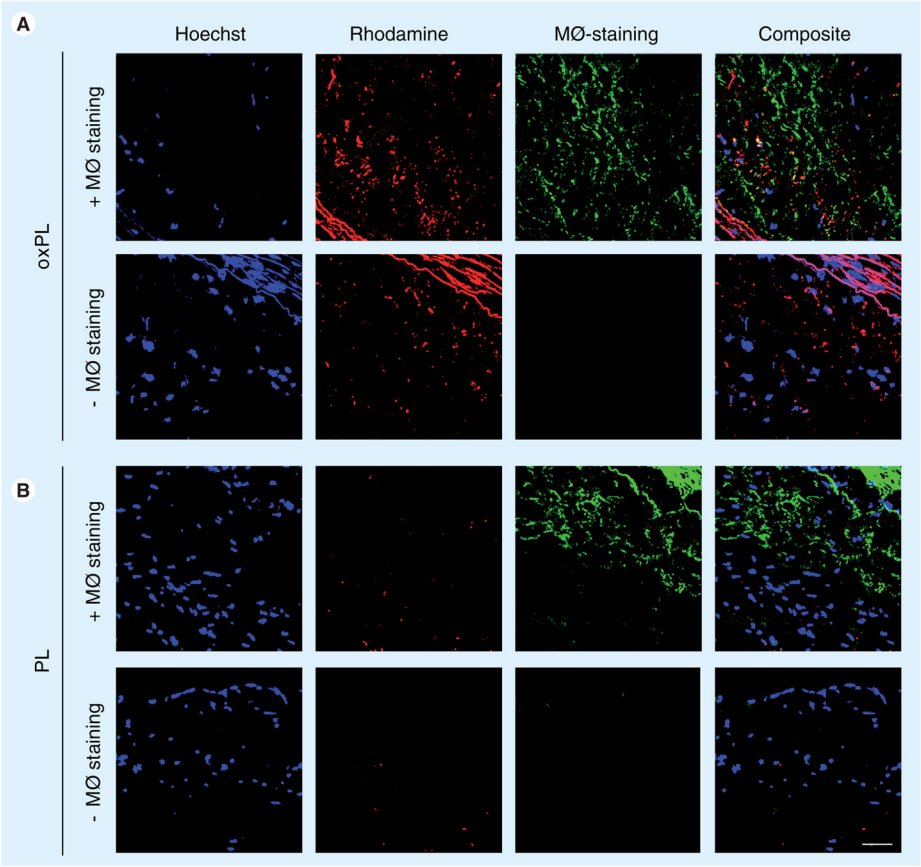

Figure 5. Confocal microscopy of atherosclerotic plaque

Tissue samples were stained with cy-5 RAM 11 antibody (green pseudocolor) directed to macrophages. In addition, macrophage staining was omitted in order to confirm that there is no overlap between the two fluorescent signals. Vesicles were detected by red rhodamine fluorescence only in oxPL-injected animals. Hoechst staining was used to visualize nuclei (blue on merged images). Merged images showed colocalization of oxPL in macrophage-rich plaque areas, appearing in yellow composite. Bar represents 50 μm.

MØ: Macrophage; oxPL: Cholesteryl-9-carboxynonanoate phospholipid vesicles; PL: Phospholipid.

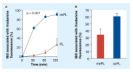

Figure 6. ***In vitro*** **study of uptake of oxPL by human macrophages (MØ) as compared with phospholipid**

Binding of rhodamine-containing vesicles to macrophages was assessed by flow cytometry and presented as percentage of cells associated with rhodamine fluorescence. **(A)** Time course of vesicle uptake by macrophages. **(B)** Binding of oxPL as compared with control vesicles containing methyl ester-modified 9-CCN.

MØ: Macrophage; oxPL: Cholesteryl-9-carboxynonanoate phospholipid vesicles; PL: Phospholipid.

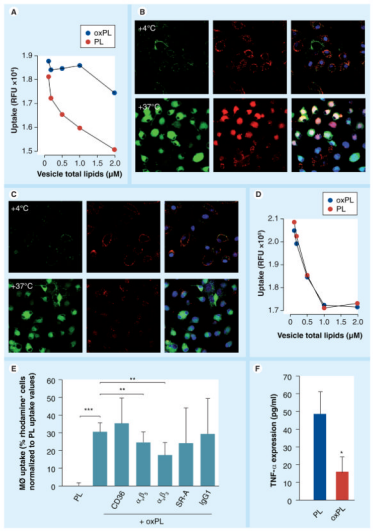

Figure 7. Uptake of low-density lipoprotein in the presence of vesicles

(A) oxPL or PL were preincubated with BODIPY-LDL for 1 h followed by exposure to cultured human macrophages and uptake was quantified as relative fluorescence units. Under confocal microscopy cells show strong uptake of BODIPY-LDL (green) and rhodamine (red) when incubated with oxPL **(B)** but not with PL **(C).** Blue is DRAQ5 nuclear staining. Uptake is reduced at 4°C. **(D)** Cultured human macrophages were incubated with oxPL or PL following treatment with DiI-acLDL. **(E)** Inhibition experiments with antibodies against macrophage uptake pathways. The level of uptake inhibition indicates potential involvement of receptors in the uptake mechanism. Cells were pretreated with corresponding antibodies and rhodamine fluorescence was quantified by flow cytometry. Values presented as normalized to PL uptake. **(F)** TNF-α expression in macrophages exposed to oxPL or PL. *$p < 0.05$; **$p < 0.0005$; ***$p < 0.001$.
LDL: Low-density lipoprotein; MØ: Macrophage; PL: Phospholipid.

Table 1

Vesicle composition, their physicochemical and MR relaxivity properties.

Vesicles	Vesicle composition (mol. % of lipid)†					Mean size (nm)	PDI	Zeta potential (mV)	r_1 at 1.5 T ($s^{-1}.mM^{-1}$)
	PC	*PS*	*9-CCN*	*Chol*	*9-CCN-OMe*				
oxPL	44.8	5.0	15.0	20.0	0.0	130	0.179	−69.95 ± 1.91	5.9 ± 0.1
PL	44.8	5.0	0.0	35.0	0.0	140	0.202	−46.92 ± 2.49	5.7 ± 0.1
mePL	44.8	5.0	0.0	20.0	15.0	112	0.671	−45.21 ± 4.33	

†All formulations contained 15 mol.% of Gd-DTPA-SA and 0.2 mol.% of rhodamine-DOPE.

mePL: (3b)-cholest-5-en-3-yl methyl azelaate phospholipid vesicles; oxPL: Cholesteryl-9-carboxynonanoate phospholipid vesicles; PC: Phosphatidylcholine; PDI: Polydispersity indices; PL: Phospholipid; PS: Phosphatidylserine.